Optics & Laser Technology 158 (2023) 108926

Contents lists available at ScienceDirect

Optics and Laser Technology

journal homepage: www.elsevier.com/locate/optlastec

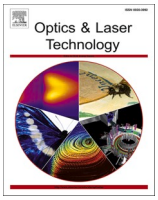

Full length article

Wireless optical power transmission based on the off-axis VECSEL of long resonator

Zhuo Zhang [a,b], Jianwei Zhang [a,*], Yinli Zhou [a], Xing Zhang [a], Jiye Zhang [a], Jun Zhang [a], Yongqiang Ning [a], Li Qin [a], Lijun Wang [a]

[a] State Key Laboratory of Luminescence and Applications, Changchun Institute of Optics, Fine Mechanics and Physics, Chinese Academy of Sciences, Changchun, Jilin 130033, China

[b] University of Chinese Academy of Sciences, Beijing 100049, China

ARTICLE INFO

Keywords:
Vertical external cavity surface-emitting laser
Laser resonator
Wireless power transmission

ABSTRACT

We present laser generation in a several-meters-long air cavity using an optically pumped semiconductor gain chip for wireless optical power transmission applications. Theoretical calculations showed that stable laser oscillation can be realized in long laser oscillation cavities of more than 500 cm. Moreover, the laser oscillation can be maintained even when the output mirror of the laser is off-axis, which is useful in the alignment of energy charging terminals. A lens was inserted into the cavity to adjust the intra-cavity beam, and the beam radius on the gain chip surface sufficiently increased to match a large pump spot and achieve high output power. Laser generation in an external air cavity of 200 cm was realized, and the maximum output laser power of more than 705.4 mW was achieved. The off-axis range of the output mirror surpassed 19 mm. Moreover, the output laser power decreased by 5.5 % (from 586.4 to 554.2 mW) when the length of the external air cavity was increased from 100 to 200 cm. However, the off-axis range increased by 40.7 % (13.5 to 19 mm). Thus, the longer external cavity laser made it easier to align the laser beam and charging terminal.

1. Introduction

Electronic devices and smartphones are convenient but require frequent charging. Carrying charging equipment and looking for power supplies to charge mobile devices create significant inconvenience for users. Therefore, efficient wireless charging technology has become a research hotspot [1–4]. Current wireless power transmission systems can be divided into three main categories: inductive coupling, magnetic resonance coupling, and microwave radiation categories [5,6]. Among these, magnetic induction and magnetic resonance coupling technologies operate in the near-field, but they have shortcomings in terms of their short charging distance and thermal effects [7–9]. However, microwave radiation technologies use microwaves for energy transmission rather than a variable magnetic field [10]. The energy transmission range of microwaves has expanded from tens of meters to several kilometers, but the associated high radio frequency (RF) density leakage is harmful to the human body, which limits its application [11–13]. With the rapid development of laser sources, such as semiconductor lasers, solid-state lasers, and solar disk lasers, laser applications in communication and space power transmission have been continuously reported [14–18]. Lasers with good directivity and high power densities are ideal light sources for wireless energy transmission. The considerable developments in laser technology are conducive for long-distance and high-efficiency wireless power transmission with light as the energy carrier [19].

In recent years, wireless charging systems using light as the energy carrier have been the research focus [20–22]. The resonant cavity of a laser offers significant advantages in wireless charging. Any occlusion that enters the resonator stops the laser output but the occlusion is not harmed. A laser with an optical gain greater than the cavity loss can output the laser in a resonant cavity with length of several kilometers [23]. By tweaking the design of the resonant cavity, its output can have a certain off-axis working range to realize mobile wireless optical power transmission [20]. As an information carrier, light can simultaneously transmit energy and information [24–27]. Therefore, a wireless power transmission system based on light has the potential for both communication and charging. The optically pumped vertical external cavity surface emitting laser (VECSEL) with high power, high beam quality,

* Corresponding author.
E-mail address: zjw1985@ciomp.ac.cn (J. Zhang).

https://doi.org/10.1016/j.optlastec.2022.108926
Received 18 August 2022; Received in revised form 8 November 2022; Accepted 11 November 2022
Available online 19 November 2022

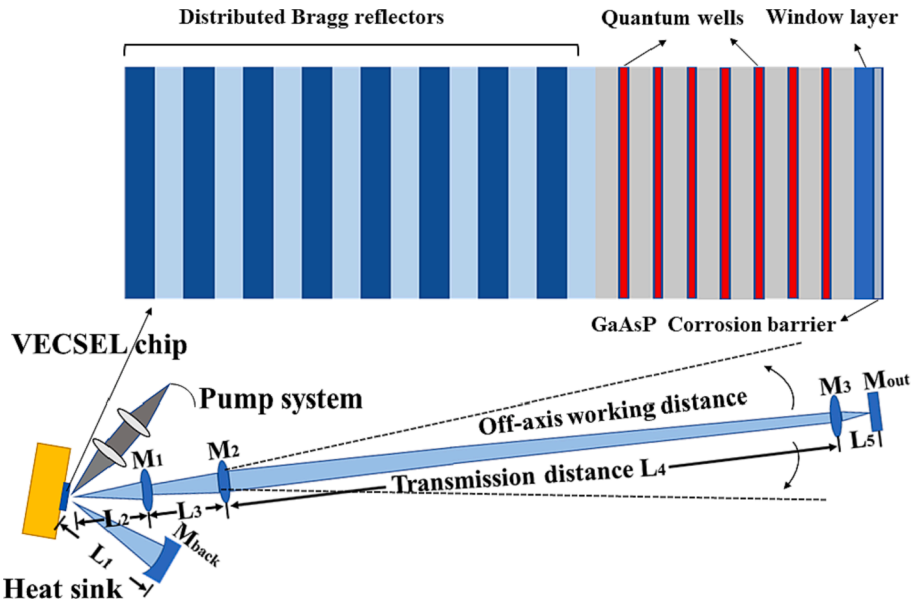

Fig. 1. Schematic diagram of the working principle in the long cavity VECSEL.

low cost, and flexible resonator is the ideal choice for wireless power transmission systems [28,29].

VECSELs combine the advantages of solid-state and gas lasers to achieve high power and high beam quality outputs [30]. Resonant cavity designs can accommodate optical elements in the cavity for frequency conversion, mode control, and mode locking [31–34]. Highly efficient intra-cavity frequency conversion combined with semiconductor material flexibility enables VECSELs to cover an emission wavelength range from the ultraviolet to long-wave infrared [35–37]. Thus, VECSELs are eminently suitable for wireless power transmission, but no current study has investigated high-power wireless power transmission systems using VECSELs, to our knowledge.

This study demonstrates a wireless power transmission scheme based on a VECSEL external cavity structure. Long-distance wireless energy transmission is realized by optimizing the beam propagation path in the resonant cavity. A V-shaped cavity structure with a transmission distance of 200 cm and an output power of 700 mW is designed by analyzing the influence of the beam radius on the gain chip surface from the output power of the laser. Additionally, the output power and off-axis characteristics of different transmission cavity lengths are analyzed.

2. System overview

Fig. 1 displays a wireless power transmission scheme based on the external cavity structure of a VECSEL, which has a V-shaped structure. A flat concave mirror, M_{back}, with a curvature radius of 77 mm and high reflectivity (>99.9 %) is used as the feedback end. The output end comprises a convex lens, M_3, and plane mirror, M_{out} (reflectivity, ~97.5 %). M_1 and M_2 modify the transmission beam in the cavity to help yield a high-power, long cavity laser output. M_1, M_2 and M_3 are convex lenses with a diameter of 25.4 mm, a radius of curvature of 15 cm and coated with an anti-reflective film (transmittance >99.9 %) to reduce intra-cavity transmission losses. By tailoring the laser cavity, the feedback end and M_1 and M_2 positions are fixed, and the output end can achieve long-distance off-axis laser oscillation. In Fig. 1, the folding angle of the V-shaped cavity is about 30°, and the incident angle of the beam on the surface of the gain chip in the cavity is about 15°.

Fig. 1 also shows the VECSEL gain chip structure. The chip has a bottom-emitting structure, while a GaAsP corrosion barrier layer, window layer, active region, and distributed Bragg reflector (DBR) are successively grown on the substrate [38]. The DBR layer of the structure is grown the last and is welded to a copper heat sink after metallization. The substrate is removed via mechanical thinning and chemical etching. The GaAsP corrosion barrier layer protects the chip from chemical corrosion. After removing the substrate of the gain chip, the copper radiator of the welded chip is installed on the copper base and cooled using a thermoelectric cooler (TEC). A water-cooling system with a set temperature of 15 ℃ is used to remove waste heat generated during TEC operations. The pump system provides an 808 nm pump light output, and the maximum pump power is 100 W. The pump laser is focused on the gain chip at an incidence angle of nearly 35° through the lens group. The size of the pump spot and the pump power density are controlled by adjusting the distance between the lens group and chip.

The gain chip is grown on GaAs (1 0 0) substrates using an Aixtron 200/4 metalorganic chemical vapor deposition system. As shown in the structural illustration of Fig. 1, the active region is grown on top of the GaAsP corrosion barrier layer and the 30-nm-thick AlGaAs window layer. The active region comprises eight 6-nm-thick InGaAs quantum wells (QWs) placed in the GaAs pump absorption layer. The 3-nm-thick GaAsP barrier layer placed on either sides of the QW compensates for the material strain caused by the InGaAs QW [39]. A highly reflective DBR is placed behind the active region, which reduces the heat deposition on the chip and increases its efficiency. Thirty-five pairs of AlAs/GaAs DBRs provide a high reflectivity of >99.9 % in the 100 nm range near the laser wavelength. Even if the light is incident at a 30° angle, the DBR still provides a reflectivity greater than 99.9 %.

The laser cavity scheme in Fig. 1 requires a precise design to support long-distance laser oscillation. The distance between M_1 and M_2 is L_3, and the distance between M_2 and M_3 is the transmission distance of L_4. M_{back} reflects the light in the cavity and focus it on the surface of the gain chip. M_1 and M_2 modify the beam size in the cavity. The spot that converges on the gain chip matches the pump light for achieving high-power output. The larger the beam size received by M_3, the larger the off-axis range. M_3 focuses the intracavity beam on M_{out}. The light reflected by M_{out} returns to the cavity through M_3 modifications. Note that a slight change in the lens position of the laser cavity affects the cavity's stability. Thus, a theoretical model is established to simulate the cavity stability to obtain an accurate laser cavity design scheme.

The laser cavity design is based on the generalized ABCD matrix method [40]. The ABCD matrix method is concise and efficient and has been widely used in the analysis and design of laser resonators and beam propagation [41,42]. By calculating the ABCD matrix transformation of

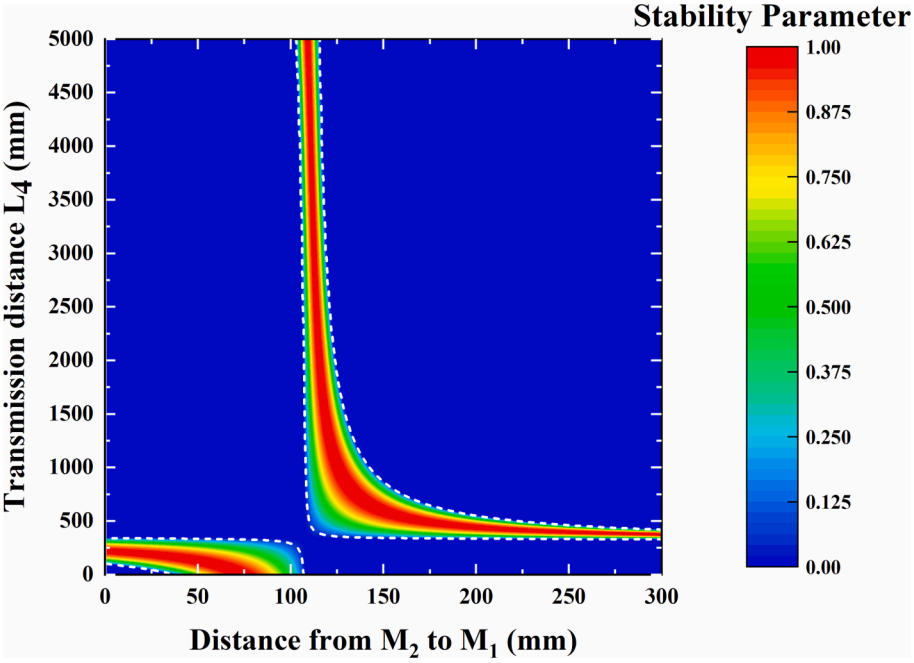

Fig. 2. Influence of the cavity lengths L_4 and L_3 in the VECSEL on the cavity stability. The area enclosed by the white dotted line is the working area for cavity stabilization.

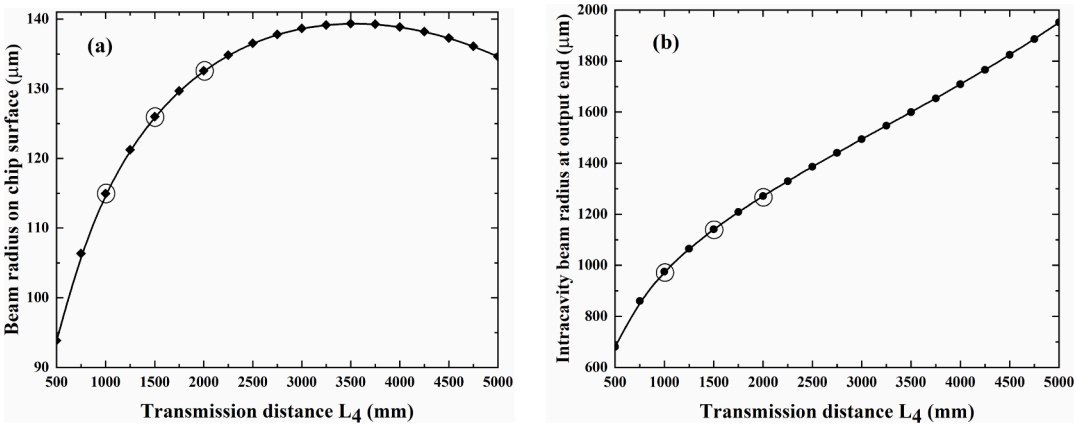

Fig. 3. (a) Beam radius on the chip surface as a function of the transmission distance, and (b) beam radius on M_3 as a function of transmission distance.

each mirror in the cavity, the beam propagation parameters for each position in the cavity are obtained. In a stable laser cavity, the laser beam must be able to oscillate multiple times without leakage. Thus, the absolute values of the stability parameters calculated using the ABCD matrix are between 0 and 1 [43]. In the calculation, the curvature radius of the three convex lenses is 15 cm. The thermal lensing effect of the semiconductor materials with a high pump temperature is about 650 mm [44]. The influence of the thermal lensing effect on the short cavity length VECSEL is negligible. With increasing cavity length, the influence of the thermal lensing effect intensifies, which cannot be ignored in the long cavity VECSEL. When calculating the beam propagation in the cavity simulated by the ABCD matrix, the position of the gain chip is no longer a plane mirror but a thermal lens with a curvature radius. To accurately calculate the beam propagation in the cavity, the gain chip position is replaced with the lens having a 650 mm curvature radius. The M_2 position is closely related to the transmission distance L_4 and off-axis range.

Fig. 2 displays the stability parameters of the laser cavity. The areas where the laser cavity cannot work stably are marked with dark blue. The distance L_3 between M_2 and M_1 is approximately 125 mm, and the transmission distance L_4 is about 5 m. When L_3 is increased, the transmission distance L_4 sharply decreases to 50 cm. Therefore, this type of laser cavity supports the stable operations of relatively long cavity lengths to achieve long-distance wireless energy transmission.

Fig. 3(a) displays the variations in the beam radius on the chip surface with increasing propagation distance. The beam radius on the gain chip increases with the propagation distance L_4. A larger intracavity beam radius on the chip surface allows a larger pump spot to be supported. A critical value exists for the size of the pump spot, which is directly related to the thermal conductivity of the heat sink and semiconductor materials [45]. Beyond this critical value, the thermal resistance of the heat sink becomes greater than that of the semiconductor material, and subsequently, the heat sink loses its heat dissipation capability. This causes a sharp increase in the temperature of the active region. Based on the critical value formula [45], the maximum pump spot radius that the gain chip can support is about 200 μm. Under the critical value of the maximum pump spot, the output power increases with the pump spot radius. As the transmission distance L_4 increases

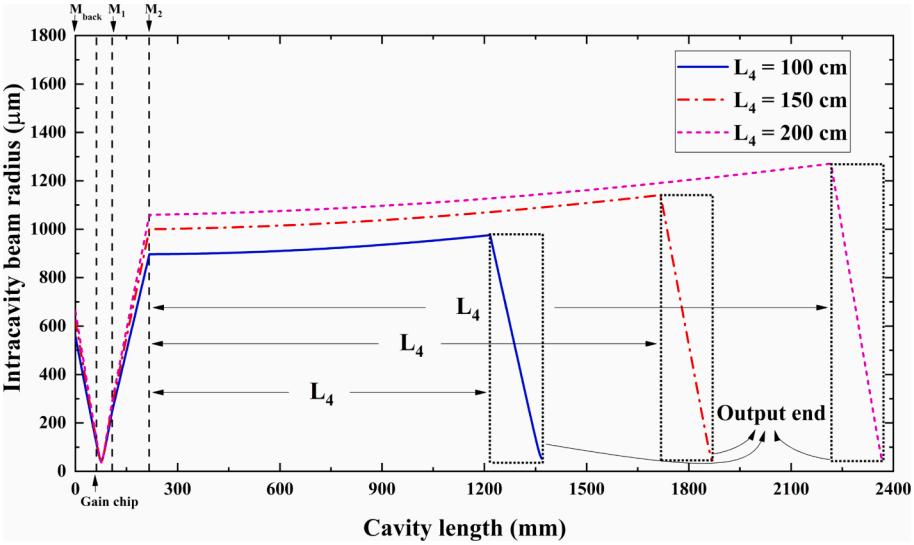

Fig. 4. VECSEL internal oscillating laser beam distribution for L_4 values of 100, 150, and 200 cm.

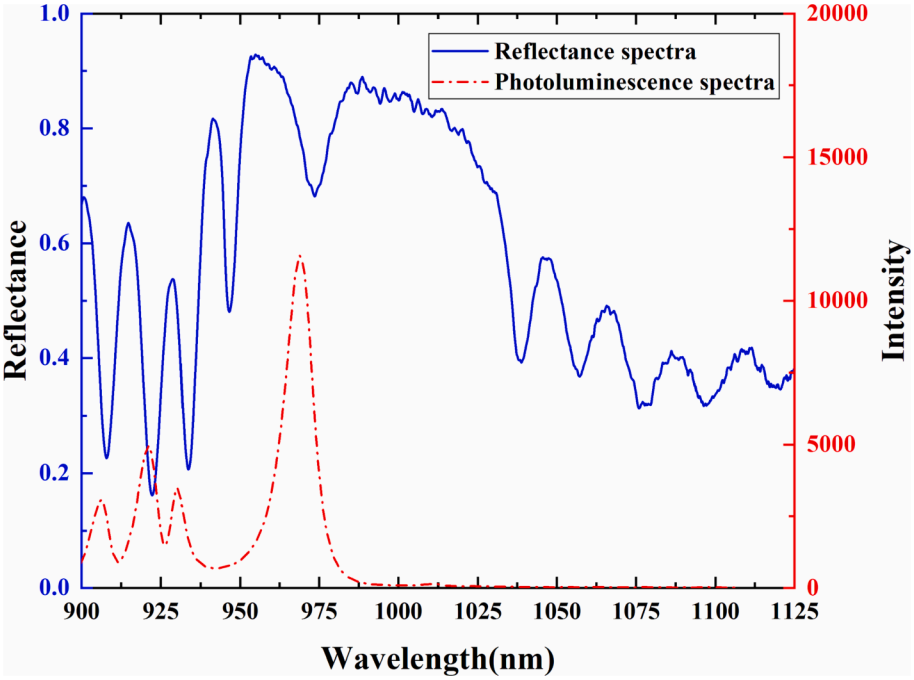

Fig. 5. The 0 °C gain chip reflection spectrum (solid line) and PL spectrum from the InGaAs chip (red dash curve). (For interpretation of the references to colour in this figure legend, the reader is referred to the web version of this article.)

from 500 to 2000 mm, the beam radius on the chip surface increases from 94 to 132 μm. Furthermore, the pump spot size that the system can support increases.

Fig. 3(b) shows how the beam radius of the M_3 surface varies with the transmission distance. The beam radius on the M_3 surface gradually increases with the propagation distance L_4. A large beam radius results in a large off-axis range. The beam reflected toward the resonant cavity by the output end composed of M_3 and M_{out} oscillates in the cavity. The condition for laser output is that the optical gain generated by the gain chip is greater than the loss. The larger the radius of the M_3 surface beam, the larger the region of the output end that deviates from the optical axis can reflect enough gain and the larger the off-axis range. As the propagation distance L_4 increases from 500 to 2000 mm, the beam radius on the M_3 surface increases from 680 to 1250 μm and the off-axis range of the output end increases. In Fig. 3(a) and 3(b), the beam radius corresponding to transmission distances of 1000, 1500, and 2000 mm are circled.

Fig. 4 displays the radius variations of the beam propagation over the entire cavity when L_4 is 100, 150, and 200 cm. To better display the beam radius distribution, the V-shaped cavity is expanded to form a linear cavity. The location of each component is marked in Fig. 4. M_1 adjusts the beam propagation so that the beam waist is not on the chip surface, which maximizes the beam radius on the chip surface.

As the cavity length increases, the beam radius on the left side of M_2 little changes. This means that a compact transmitter can be fabricated by selecting appropriate lens specifications. The output terminal composed of M_3 and M_{out} is circled in a black dotted box in Fig. 4. As the propagation distance increases, the beam propagation inside the output

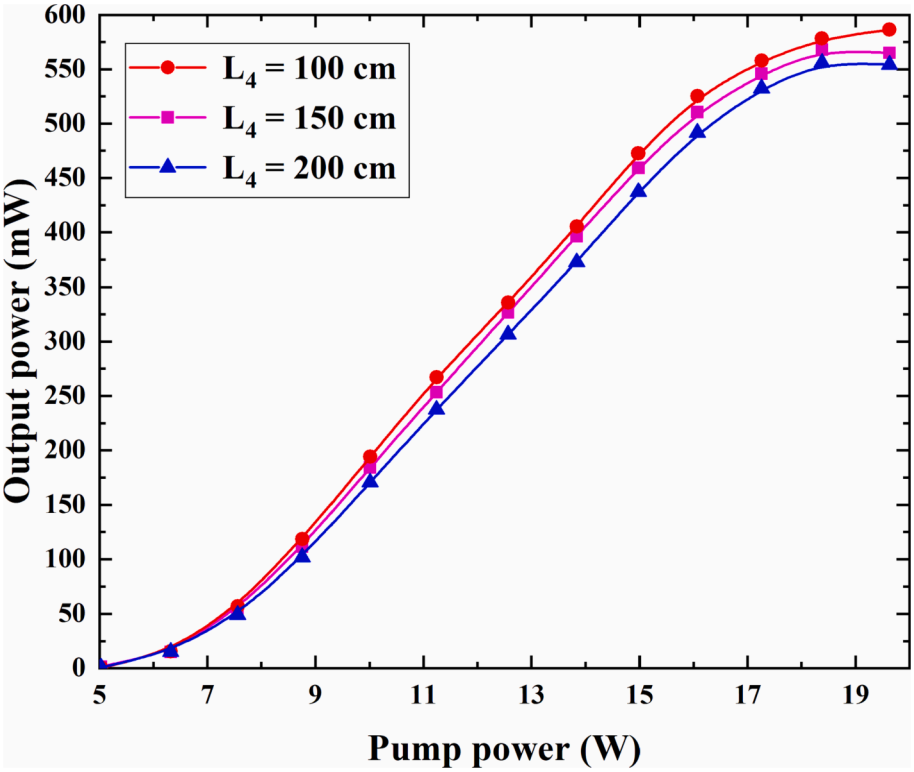

Fig. 6. VECSEL output power curves for different external cavity lengths at 0 °C.

end stabilizes and the beam radius on the M_{out} surface is about 50 μm. The output end can be fabricated as a movable compact module. In wireless energy transmission systems, a compact transmitter and movable output end without the need for debugging will provide significant advantages.

3. Experiment

We designed a V-shaped cavity that could work stably in a long cavity, as shown in Fig. 1. The gain chip structure is grown on GaAs (100) substrates, and the wafer is cut to 3 × 3 mm^2. For better heat removal, the gain chip is soldered to a copper heat sink. The reflectivity

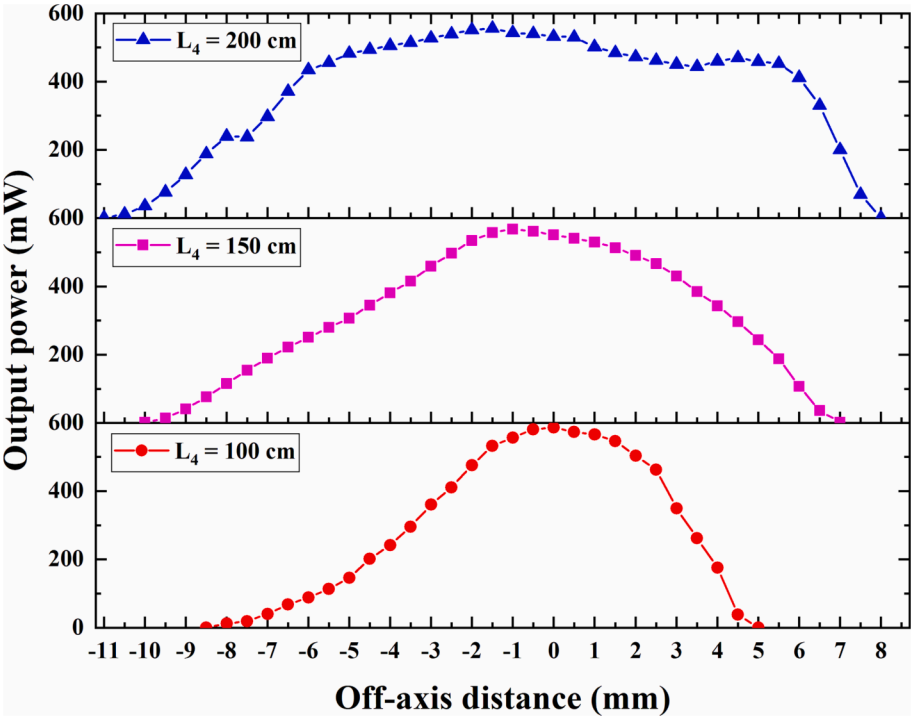

Fig. 7. VECSEL output power as a function of the off-axis distance for different cavity lengths (L_4 = 100, 150, and 200 cm). An off-axis distance of zero indicates that the central axis of the output mirror group matches the central axis of the VECSEL system.

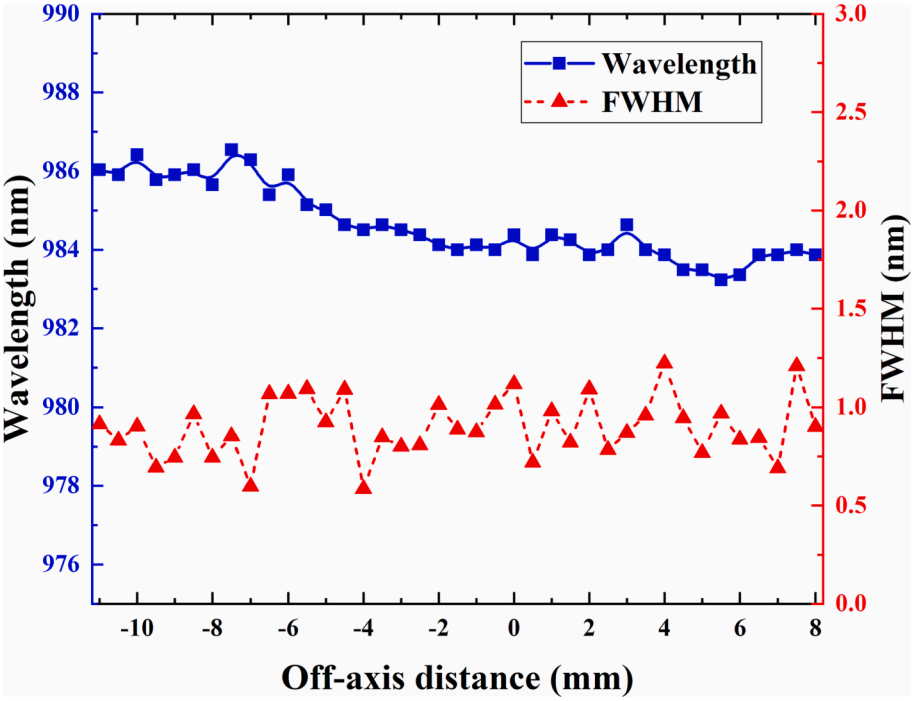

Fig. 8. VECSEL laser wavelength and spectral half-width for different off-axis distances with L_4 = 200 cm.

and photoluminescence (PL) spectra at room temperature after the removal of the substrate are shown in Fig. 5. The dip in reflectance indicates that the wavelength of the F-P resonances is 974 nm. The peak of the PL spectra as modified by the microcavity is 968 nm. The temperature drift rate of the gain peak with high temperatures is about 3 times faster than that of the cavity mode with a temperature rise [38]. Therefore, increases in the active region temperature improve the match between the gain peak and cavity mode, which yields optimal outputs.

Fig. 6 shows the output power as a function of pump power for different transmission distances of L_4 (100, 150, and 200 cm) with a heat-sink temperature of 0 ℃. Here, the position parameters of the optical lens in the VECSEL scheme are similar to those simulated in Fig. 4. The distance between M_{back} and chip L1 is about 6.5 cm, that between the chip and M_1 is about 4.5 cm, that between M_1 and M_2 is about 10 cm, and that between M_3 and M_{out} is about 15.5 cm. The linear dependence range of the output power on the pump power and the output power rollover caused by excessive pump power is observed. With increasing pump power, the output power increases until thermal rollover. The main reason for thermal rollover is that the pump power of the laser is too high, and the radiator cannot dissipate the heat in time. Therefore, a sharp rise in the heat storage temperature for the active region leads to a mismatch between the PL red-shift and the FP cavity mode, which decreases the output power. Fig. 6 shows that as the transmission distance increases, the peak output power slightly decreases. The cavity loss increases with the transmission distance. As shown in Fig. 6, the power reduction decreases with increasing cavity length. The intracavity beam radius on the chip surface gradually increases with the transmission distance, as shown in Fig. 3(a). As the transmission distance L_4 increases from 100 to 200 cm, the spot radius on the chip surface gradually increases from 115 to 132 μm. The pump spot radius is fixed as 135 μm. The pump position and pump power are fixed. The intracavity beam radius on the chip surface increases with the transmission distance L_4 to better match the pump spot, and the output power slightly increases. A small increase in the output power can offset some of the loss from the increased cavity length. Thus, the power attenuation is very low. As the cavity length increases from 100 to 200 cm, the maximum output power of the VECSEL decreases from 586.4 to 554.2 mW. The power attenuation caused by the increase of the transmission distance is about 5.5 % per meter, indicating that the scheme can support wireless optical power transmission with a transmission distance of several meters.

Off-axis operations of the laser are experimentally verified, as shown in Fig. 7. The output end (M_3 and M_{out}) moves in a plane perpendicular to the optical axis in the off-axis operation. Note that the positions of M_{back}, chip, M_1, M_2, and pump system are not changed in the experiments of the increase of L_4 distance and output end (M_3 and M_{out}) off-axis working. Based on the data in Fig. 3(b), the beam radius at the output end gradually increases with the transmission distance L_4. The structure of the output end plays an essential role. The output end deviates from the optical axis, and the beam is reflected according to the incident path to form a stable resonance. The threshold condition of the VECSEL output is that the gain in the cavity is greater than the loss in the cavity. The beam radius on the M_3 surface is large, signifying that the output end comprising M_3 and M_{out} can move in a plane perpendicular to the optical axis until the gain of the feedback beam is less than the loss in the cavity and VECSEL stops the output. In Fig. 7, the abscissa is zero, which denotes that the output end is aligned with the optical axis of the other optical elements. As shown in Fig. 7, the translation range is about 19 mm when the transmission distance L_4 is 200 cm. At the off-axis edge position, the optical gain of the output end feedback is less than the cavity loss, and the laser stops the output. As the transmission distance increases from 100 to 200 cm, the off-axis range increases from 13.5 to 19 mm. The increased off-axis range is related to the increased beam radius on the M_3 surface in Fig. 3(b). With increasing cavity length, the beam radius received by the output end gradually increases and the off-axis range steadily increases. The transmission distance L_4 is 200 cm, and the output end still has 20 % of the peak laser power output in the range of − 9 to 7 mm. The off-axis range can be extended and the appropriate lens can be chosen to reduce the size of the output end. One transmitter can support the simultaneous output of multiple output terminals. Thus, multiple devices can be simultaneously charged on a wireless power transmission system.

Fig. 8 shows the output wavelength and full width at half maximum (FWHM) of VECSEL for different off-axis distances. In the off-axis region, the output wave increases from 983.2 to 986.3 nm. The corresponding laser spectral half-width fluctuates between 0.5 and 1.5 nm. As shown in Fig. 1, the inward translation of the output end perpendicular to the

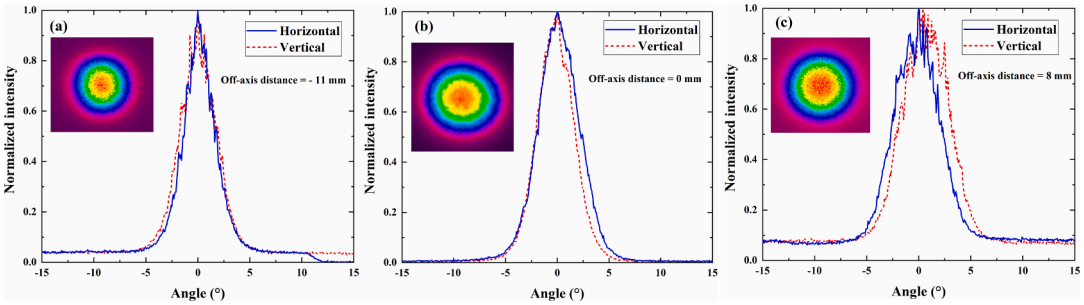

Fig. 9. One-dimensional far-field patterns of VECSEL measured for different off-axis working ranges: (a) −11 mm, (b) 0 mm, and (c) 8 mm. Inserts display the beam profiles from VECSEL.

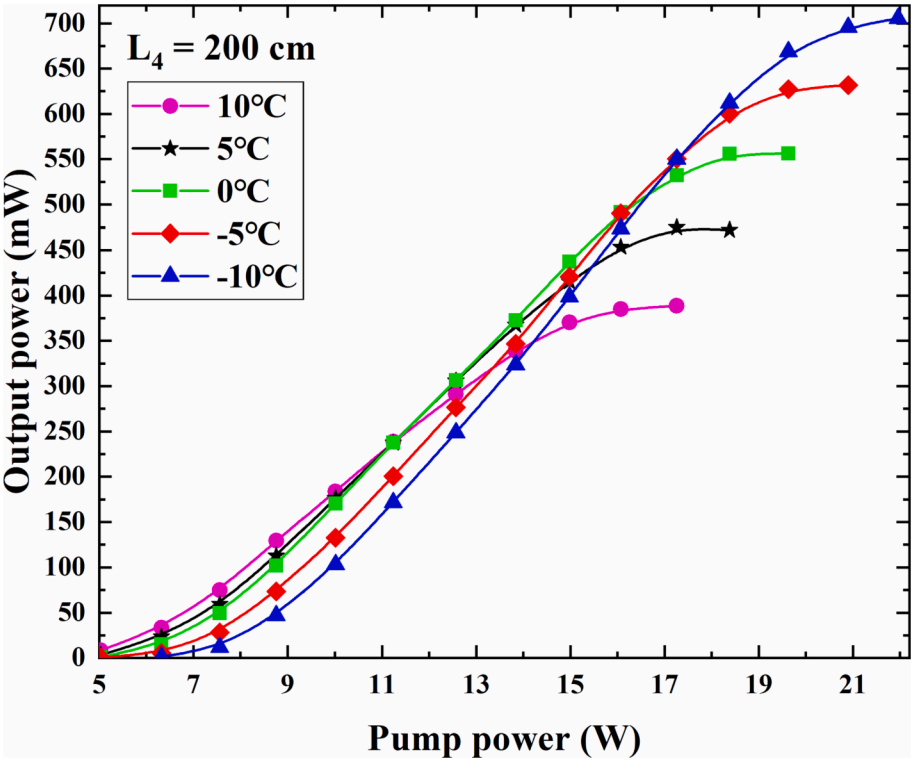

Fig. 10. VECSEL output power curve for an external cavity length of 200 cm and different operating temperatures.

optical axis is recorded as negative coordinates, and the outward translation is recorded as positive coordinates. With increasing distance from − 11 to 8 mm, the angle of the V-shaped cavity gradually increases. Subsequently, the photon energy increases, which results in a blue shift of the wavelength [46].

Fig. 9 shows the far-field of VECSEL at 0 °C with a transmission distance of 200 cm and an off-axis working distance of − 11, 0, and 8 mm. The far-fields at different positions show the Gaussian cross sections in the horizontal and vertical dimensions. The beam intensity is too high when the optical axis is aligned, and an attenuator is added to the measurements. When the beam intensity is weak at the off-axis edge, the attenuator is removed and the focal length of the detector is adjusted during measurements. Thus, the 2D beam profiles can be observed. The divergence angle is measured at $1/e^2$ of the maximum beam intensity. At the off-axis positions of − 11, 0, and 8 mm, the divergence angles are 7.677°, 7.248°, and 7.901°, respectively.

Fig. 10 shows the effect of the heat-sink temperature on the VECSEL power curve when the transmission distance L_4 is 200 cm. The figure displays the linear dependence range of the output power on the pump power and the output power reversal caused by high pump power. As the heat sink temperature decreases, the pump power required for thermal rollover increases and the output peak power increases. Thermal rollover primarily occurs due to a mismatch between the PL redshift and FP cavity mode from the high internal temperature of the chip. At the transmission distance of 200 cm, a maximum output power of 705.5 mW is realized at a heat-sink temperature of −10°C.

4. Conclusions

In this study, we used the ABCD matrix method to simulate the stability of a laser cavity for designing and verifying a wireless optical power transmission scheme based on VECSEL. Through design, a stable laser cavity of more than 5 m was realized. The beam radius in the cavity was simulated as a function of the propagation distance. The beam sizes on the left and right sides of the transmission distance L_4 remained nearly unchanged, and they could be fixed onto the compact emission and output ends by selecting appropriate optical component specifications. An intracavity lens was inserted into the cavity to adjust the intracavity beam so that the beam waist increased on the gain chip surface. The gain chip surface beam radius became large enough to

support a large pump spot and realize a high output power. The maximum output power of 705.4 mW was obtained at a transmission distance of 200 cm. The output end had a working range of 19 mm away from the optical axis. The laser beam exhibited a Gaussian spot morphology, and the beam divergence angle was only 6.87°. Based on the small size and low cost of semiconductor lasers, we believe that the proposed compact, wireless, optical power transmission system has considerable potential. Such a long resonant cavity is conducive for adding optical elements for modulation to facilitate the simultaneous transmission of energy and information.

Declaration of Competing Interest

The authors declare that they have no known competing financial interests or personal relationships that could have appeared to influence the work reported in this paper.

Data availability

Data will be made available on request.

Acknowledgements

This work was supported by the National Key Research and Development Program of China (Grant no. 2018YFB2201103); the Major Program of National Natural Science Foundation of China (Grant no. 62090060); and the National Natural Science Foundation of China (Grant nos. 61874117, 61874119, 11774343, and 61804087).

References

[1] L. Han, L.M. Li, Integrated wireless communications and wireless power transfer: An overview, Phys. Commun. 25 (2017) 555–563.
[2] K.W. Choi, A.A. Aziz, D. Setiawan, N.M. Tran, L. Ginting, D.I. Kim, Distributed wireless power transfer system for internet of things devices, IEEE Internet Things J. 5 (2018) 2657–2671.
[3] X. Lu, D. Niyato, P. Wang, D.I. Kim, Z. Han, Wireless charger networking for mobile devices: Fundamentals, standards, and applications, IEEE Wirel. Commun. 22 (2015) 126–135.
[4] Q. Liu, J. Wu, P. Xia, S. Zhao, L. Hanzo, Charging unplugged: Will distributed laser charging for mobile wireless power transfer work? IEEE Trans. Veh. Technol. 11 (2016) 36–45.
[5] S. Li, C.C. Mi, Wireless power transfer for electric vehicle applications, IEEE J. Emerg. Sel. Top Power Electron 3 (2014) 4–17.
[6] N. Shinohara, Wireless power transmission: Inductive coupling, radio wave, and resonance coupling, in: D.L. Peter, B. John, H. Reinhard, F. Damian (Eds.), Advances in Energy Systems: The Large-scale Renewable Energy Integration Challenge, Wiley Online Library, Hoboken, 2019, pp. 211–220.
[7] D. Alashgar, K. Fujiwara, N. Nagaoka, Fundamental investigation of short-range inductive coupling wireless power transmission by using series-series capacitive compensation topology, J. Asian Electr. Veh. 17 (2019) 1811–1822.
[8] M.F. Haider, M.M. Hassan, S. Ahmad, F. You, Wireless power transmission based on magnetic resonance coupling, International Conference on Electrical, Communication, and Computer Engineering. IEEE (2019) 1–3.
[9] G.J. Gwon, Y. Kwon, Enhancement of wireless power transmission efficiency and flexibility via an optimized three-dimensional coupled magnetic resonance system with double transmitter coil, J. Electr. Eng. Technol. 16 (2021) 1415–1426.
[10] M.V. Reddy, K.S. Hemanth, C.H.V. Mohan, Microwave power transmission—a next generation power transmission system, IOSR J. Electr Electron Eng 4 (2013) 24–28.
[11] B. Strassner, K. Chang, Microwave power transmission: Historical milestones and system components, Proc. IEEE 101 (2013) 1379–1396.
[12] F. Zhao, L. Wei, H. Chen, Optimal time allocation for wireless information and power transfer in wireless powered communication systems, IEEE T. Veh. Technol. 65 (2015) 1830–2185.
[13] N. Shinohara, The wireless power transmission: Inductive coupling, radio wave, and resonance coupling, Wiley Interdiscip Rev. Energy Environ. 1 (2012) 337–346.
[14] C. Zhao, H. Zhang, Z. Guan, et al., Solar pumped lasers for free space laser communication, Photoptics (2019) 268–275.
[15] K. Iga, J. Tatum, Single-mode VCSELs for communications applications, Communication and Sensing, VCSEL Industry, 2021, p. 189.
[16] Y. Jiang, Y.Y. Liu, X. Liu, et al., Organic solid-state lasers: A materials view and future development, Chem. Soc. Rev. 49 (16) (2020) 5885–5944.
[17] D. Garcia, D. Liang, C.R. Vistas, et al., Ce: Nd: YAG solar laser with 4.5% solar-to-laser conversion efficiency, Energies (2022;15(14):5292.).
[18] J. Almeida, D. Liang, D. Garcia, et al., 40 W continuous wave Ce: Nd: YAG solar laser through a fused silica light guide, Energies 15 (11) (2022) 3998.
[19] J. Ding, W. Liu, C. Lin, H. Zhang, H. Mei, Advanced progress of optical wireless technologies for power industry: An Overview, Appl. Sci. 10 (2020) 6463.
[20] J. Lim, T.S. Khwaja, J. Ha, Wireless optical power transfer system by spatial wavelength division and distributed laser cavity resonance, Opt. Express 27 (2019) A924–A935.
[21] P. Xu, W. Zhang, Z. He, Light field optimization for optical wireless power transfer, IEEE Photon J. 13 (2020) 1–9.
[22] D.H. Nguyen, T. Matsushima, C. Qin, C. Adachi, Toward thing-to-thing optical wireless power transfer: Metal halide perovskite transceiver as an enabler, Front. Energy Res. 9 (2021), 679125.
[23] G.J. Linford, W.H. Lowell, Nd:YAG long lasers, Appl. Opt. 13 (1974) 1387–1394.
[24] M. Xiong, Q. Liu, M. Liu, X. Wang, H. Deng, Resonant beam communications with photovoltaic receiver for optical data and power transfer, IEEE Trans. Commun. 68 (2020) 3033–3041.
[25] A. Minotto, P.A. Haigh, Ł.G. Łukasiewicz, E. Lunedei, D.T. Gryko, I. Darwazeh, et al., Visible light communication with efficient far-red/near-infrared polymer light-emitting diodes, Light Sci. Appl. 9 (2020) 1–11.
[26] I. Tavakkolnia, L.K. Jagadamma, R. Bian, P.P. Manousiadis, S. Videv, G. A. Turnbull, et al., Organic photovoltaics for simultaneous energy harvesting and high-speed MIMO optical wireless communications, Light Sci. Appl. 10 (2021) 1–11.
[27] A. Mansour, R. Mesleh, M. Abaza, New challenges in wireless and free space optical communications, Opt. Lasers Eng. 89 (2017) 95–108.
[28] J.E. Hastie, S. Calvez, M.D. Dawson, T. Leinonen, A. Laakso, J. Lyytikainen, M. Pessa, High power CW red VECSEL with linearly polarized TEM00 output beam, Opt. Express 13 (2005) 77–81.
[29] L. Hua, B. Zhuang, Y. Zhang, et al., Optimization of the output performance of optically pumped semiconductor disk lasers, Opt. Laser Technol. 150 (2022), 107971.
[30] A. Rahimi-Iman, Recent advances in VECSELs, J. Opt. 18 (2016), 093003.
[31] C.A. Zaugg, S. Gronenborn, H. Moench, et al., Absorber and gain chip optimization to improve performance from a passively mode locked electrically pumped vertical external cavity surface emitting laser, Appl. Phys. Lett. 104 (2014), 121115.
[32] E. Kantola, T. Leinonen, S. Ranta, et al., High-efficiency 20 W yellow VECSEL, Opt. Express 22 (2014) 6372–6380.
[33] M. Gaafar, C. Möller, M. Wichmann, et al., Harmonic self-mode-locking of optically pumped semiconductor disc laser, Electron. Lett. 50 (2014) 542–543.
[34] B.W. Tilma, M. Mangold, C.A. Zaugg, S.M. Link, D. Waldburger, A. Klenner, et al., Recent advances in ultrafast semiconductor disk lasers, Light Sci. Appl. 4 (2015) e310.
[35] M. Kuznetsov, VECSEL semiconductor lasers: A path to high-power, quality beam and UV to IR wavelength by design, Wiley Online Library, 2010.
[36] V.M. Korpijärvi, E.L. Kantola, T. Leinonen, et al., Monolithic GaInNAsSb/GaAs VECSEL operating at 1550 nm, IEEE J. Sel. Top. Quantum Electron. 21 (2015) 480–484.
[37] T. Schwarzbäck, H. Kahle, M. Eichfelder, W.M. Schulz, P. Michler, Generation of UV laser light via intra-cavity frequency doubling of an AlGaInP-VECSEL, In CLEO/Europe and EQEC 2011 Conference Digest, OSA Technical Digest (CD) (Optica Publishing Group, 2011), paper CB6_2.
[38] A.C. Tropper, S. Hoogland, Extended cavity surface-emitting semiconductor lasers, Prog. Quantum Electron. 30 (2006) 1–43.
[39] E. Kantola, T. Leinonen, S. Ranta, et al., High-efficiency tunable yellow-orange VECSEL with an output power of 20 W, Proc SPIE 8966 (2014) 89660D.
[40] S. Binghua, X. Junwen, S. Lu, Z. Huiyuan, P. Xuedan, Generalised ABCD matrix treatment for laser resonators and beam propagation, Opt. Laser Technol. 43 (2011) 1318–1320.
[41] A. Choubey, S. Mondal, R. Singh, et al., Generation of 415 W of p-polarized output power in long pulse operation of Nd: YAG laser using z-fold resonator geometry, Opt. Laser Technol. 60 (2014) 41–48.
[42] S. Khan-Afshar, U. Siddique, M.Y. Mahmoud, et al., Formal analysis of optical systems, Math. Comput. Sci. 8 (2014) 39–70.
[43] B. Tromborg, J. Osmundsen, H. Olesen, Stability analysis for a semiconductor laser in an external cavity, IEEE J. Quantum Electron. 20 (1984) 1023–1032.
[44] A.J. Kemp, J.M. Hopkins, A.J. Maclean, et al., Thermal management in 2.3-μm semiconductor disk lasers: A finite element analysis, IEEE J. Quantum Electron. 44 (2008) 125–135.
[45] R. Haring, R. Paschotta, A. Aschwanden, et al., High-power passively mode-locked semiconductor lasers, IEEE J. Quantum Electron. 38 (2002) 1268–1275.
[46] C. Hessenius, M. Lukowski, J. Moloney, et al., Wavelength tuning of VECSELs by cavity geometry, in: Vertical External Cavity Surface Emitting Lasers (VECSELs) II, 8242, SPIE, 2012, pp. 68–75.